

## Journal Pre-proofs

### Research papers

Estimation of component contributions to total terrestrial water storage change in the Yangtze River basin

Nengfang Chao, Taoyong Jin, Zuansi Cai, Gang Chen, Xianglin Liu, Zhengtao Wang

PII: S0022-1694(20)31122-7  
DOI: <https://doi.org/10.1016/j.jhydrol.2020.125661>  
Reference: HYDROL 125661

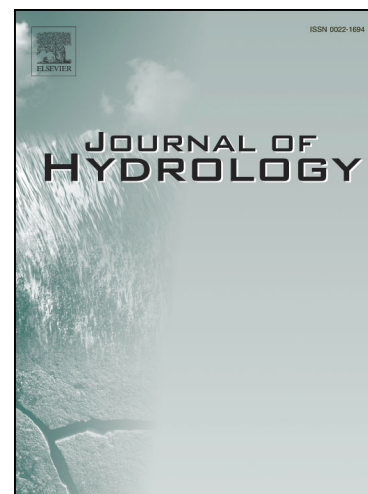
To appear in: *Journal of Hydrology*

Received Date: 9 June 2020  
Revised Date: 9 September 2020  
Accepted Date: 14 October 2020

Please cite this article as: Chao, N., Jin, T., Cai, Z., Chen, G., Liu, X., Wang, Z., Estimation of component contributions to total terrestrial water storage change in the Yangtze River basin, *Journal of Hydrology* (2020), doi: <https://doi.org/10.1016/j.jhydrol.2020.125661>

This is a PDF file of an article that has undergone enhancements after acceptance, such as the addition of a cover page and metadata, and formatting for readability, but it is not yet the definitive version of record. This version will undergo additional copyediting, typesetting and review before it is published in its final form, but we are providing this version to give early visibility of the article. Please note that, during the production process, errors may be discovered which could affect the content, and all legal disclaimers that apply to the journal pertain.

© 2020 Published by Elsevier B.V.



## **Estimation of component contributions to total terrestrial water storage change in the Yangtze River basin**

Nengfang Chao<sup>1</sup>, Taoyong Jin<sup>2, 3\*</sup>, Zuansi Cai<sup>4</sup>, Gang Chen<sup>1</sup>, Xianglin Liu<sup>1</sup>, Zhengtao Wang<sup>2, 3</sup>

1 Hubei Key Laboratory of Marine Geological Resources, China University of Geosciences, Wuhan 430074, China;

2 School of Geodesy and Geomatics, Key Laboratory of Geospace Environment and Geodesy, Wuhan University, Wuhan 430079, China;

3 Collaborative Innovation Center of Geospatial Technology, Wuhan University, Wuhan 430079, China;

4 School of Engineering and the Built Environment, Edinburgh Napier University, Edinburgh EH10 5DT, UK.

\* Correspondence: tyjin@sgg.whu.edu.cn.

**Abstract:** Terrestrial water storage (TWS) is a key variable in global and regional hydrological cycles. In this study, the TWS changes in the Yangtze River Basin (YRB) were derived using the Lagrange multiplier method (LMM) from Gravity Recovery and Climate Experiment (GRACE) data. To assess TWS changes from LMM, different GRACE solutions, different hydrological models, and in situ data were used for validation. Results show that TWS changes from LMM in YRB has the best performance with the correlation coefficients of 0.80 and root mean square error of 1.48 cm in comparison with in situ data. The trend of TWS changes over the YRB increased by  $10.39 \pm 1.27 \text{ Gt yr}^{-1}$  during the 2003–2015 period. Moreover, TWS change is disintegrated into the individual contributions of hydrological components (i.e., glaciers, surface water, soil moisture, and groundwater) from satellite data, hydrologic models, and in situ data. The estimated changes in individual TWS components in the YRB show that (1) the contribution of glaciers, surface water, soil moisture, and groundwater to total TWS changes is 15%, 12%, 25% and 48%, respectively; (2) Geladandong glacier melt from CryoSat-2/ICESat data has a critical effect on TWS changes with a correlation coefficients of  $-0.51$ ; (3) the Three Gorges Reservoir Impoundment has a minimal effect on surface water changes (mainly lake water storage), but it has a substantial effect on groundwater storage (GWS), (4) the Poyang and Doting Lake water storage changes are mainly caused by climate change, (5) soil moisture storage change is mainly influenced by surface water, (6) human-induced GWS changes accounted for approximately half of the total GWS. The results of this study can provide valuable information for decision-making in water resources management.

**Keywords:** Terrestrial water storage change; Groundwater; Yangtze River basin; GRACE;

CryoSat-2/ICESat

Journal Pre-proofs

## 1. Introduction

Terrestrial water storage (TWS) has significant ecological, environmental, societal, and economic impacts (Ramillien et al., 2008). TWS changes can also help to understand how climate change shapes global water cycles (Long et al., 2014). The Gravity Recovery and Climate Experiment (GRACE) mission (Tapley et al., 2004) has proven to be a valuable tool for detecting TWS changes (e.g., Anyah et al., 2018; Scanlon et al., 2018). As the length of GRACE data has increased over recent years, the processing of inter-satellite range-rate measurements (Watkins et al., 2015) and the background modeling of gravity change resulting from atmospheric and oceanic changes has improved significantly (Peltier et al., 2015), thereby making GRACE data more appropriate for investigating TWS changes.

The Yangtze River Basin (YRB) has a drainage area of ~1.8 million km<sup>2</sup> (~20% of the area of mainland China). It originates from the Tuotuo River in the Tanggula Range of Qinghai-Tibet Plateau (QTP), traverses 11 provinces and cities from west to east and finally discharges into the East China Sea (Figure 1). YRB has the largest reservoir in China, the Three Gorges Reservoir (TGR), as well as several large lakes, including the Poyang Lake and Doting Lake, the first and second largest freshwater lakes in China, respectively (Chen 2020a). YRB also has been the location of recent multi-billion-dollar water resource projects (e.g., Three Gorges River (TGR) and the South-North Water Diversion Project). These human activities have significantly changed river flow regimes as well as water exchanges between land, atmosphere and ocean (Chen 2020b). YRB now is an important cultural and socioeconomic region in China and plays an important role in ecological conservation. Therefore, changes in TWS and its individual component (including

glaciers, surface water, soil moisture, and groundwater) over the YRB should be investigated.

Although numerous GRACE studies on YRB can be found in the literature (e.g., Yin and Li, 2001; Ferreira et al., 2013; Huang et al., 2014; Huang et al., 2015; Long et al., 2015; Zhang et al., 2015; Jiang et al., 2016; Sun et al., 2017; Zhou et al., 2017; Chao et al., 2017a; Sun et al., 2018; Zhang et al., 2018a, 2018b; Zhang et al., 2019; Ferreira et al., 2020), most of them have focused on studying the historical flood and drought events that occurred in the YRB. A comprehensive compilation of previous GRACE studies in the YRB is summarized in Table 1. Only few of studied have focused on investigating different TWS components and the interactions between them, as well as associated hydrologic fluxes. Hasan et al. (2020) investigated the spatial drive of different TWS components to total TWS over the Nile River Basin.

In this study, we analyzed TWS components in the YRB by disintegrating TWS into the individual contributions of glaciers, surface water, soil moisture, and groundwater, based on the combination of multiple-sourced datasets collected from satellite remote sensing, large-scale hydrologic models and in situ measurements. The main contributions of this study are follows:

- (1) TWS changes were inferred from (2003–2015) monthly GRACE data using the Lagrange Multiplier Method (LMM) (Section 3.1) and validated against different GRACE solutions, different hydrological models, and in situ measurements (Section 3.1 and 4.1).
- (2) TWS changes were disintegrated into (i) glacier mass change (GMC) in the Geladandong (Section 3.2 and 4.2.1), (ii) Three Gorges Reservoir impoundment (TGRI) water storage (Section 4.2.2), (iii) lakes water storage (LWS) (Section 4.2.3), (iv) soil moisture (SM) (Section 4.2.4), and (v) groundwater storage (GWS) (Section 4.2.4). GWS changes can

further be disintegrated into human-induced groundwater storage (HGWS) and climate-driven groundwater storage anomaly (CGWS) (Section 4.2.4).

- (3) The contributions of individual TWS components to total TWS were quantified (Sections 3.3 and 4.2).
- (4) The dynamic relationships between individual TWS components were investigated (Section 4.3).

The remainder of this paper is organized as follows. Section 1 is the Introduction. Section 2 describes the utilized datasets; Section 3 introduces the methodology; Section 4 presents and discusses the results, and Section 5 summarizes the findings of the individual components contributions to total TWS over the YRB.

## **2. Datasets**

### **2.1. GRACE data**

To cross-validate TWS change, nine different GRACE TWS datasets were used in this study as detailed in the following:

- (1) The GRACE Level-two (L2) products (RL06 time-variable gravity field model) provided by the Jet Propulsion Laboratory (JPL) were used to infer TWS changes. The GRACE monthly gravity field models include a set of spherical harmonic coefficients of the fully normalized external Earth gravity field (Heiskanen et al., 1967) up to degree ( $l$ ) and order ( $m$ ) 60. The second-order terms of the GRACE time-variable gravity field model were determined from the satellite laser-ranging observational data (Cheng et al., 2011). The degree-one harmonic coefficients (Earth's geocenter) were estimated from Swenson et al. (2008), and the correction

for the glacial isostatic adjustment (GIA) was made following the procedures of A et al. (2013).

(2) GRACE TWS data were also obtained from GRGS (Groupe de Recherche de Géodésie Spatiale, etc.), of which the DDK5 filtering technique (Kusche et al., 2009) has been applied to four GRACE L2 products from the Center for Space Research (CSR), GeoForschungsZentrum Potsdam (GFZ), JPL, and GRGS.

(3) In addition, GRACE TWS data from the JPL FAN filter (Zhang et al., 2009), JPL Mascon Release 06 (Wiese et al., 2018), CSR Mascon Release 06 (Save 2020), and Goddard Space Flight Center mascons (GSFC) (Luthcke et al., 2013) mascons were also used for comparison purposes.

## **2.2. Precipitation, Evapotranspiration, and Runoff from different products**

Precipitation (P) data were derived from the Level-3 monthly of the Tropical Rainfall Measuring Mission (TRMM) with a spatial resolution of  $0.25^{\circ} \times 0.25^{\circ}$  (Huffman et al., 2007), Global Precipitation Climatology Project (GPCP) (Adler et al., 2003) with a monthly and spatial resolution of  $2.5^{\circ} \times 2.5^{\circ}$ , and China Ground Climate daily observation Data (CGCD) (<http://data.cma.cn>) with a total of 224 meteorological stations distributed over the YRB (Figure 1). Evapotranspiration (ET) data were collected from multiple sources, including four GLDAS models, the MODIS (Moderate Resolution Imaging Spectroradiometer, Mu et al., 2007), and CGCD. Runoff (R) data were taken from the Datong hydrological station in the YRB, which contains P, ET and R data.

### 2.3. Model data

- (1) **NCAR-CLM4.0 and WGHM:** The simulation data of soil moisture, snow, vegetation canopy storage, river water storage, and groundwater (2003–2015) from the NCAR-CLM4.0 (Bonan et al., 2011) were used in this study. The WaterGAP Global Hydrology Model (WGHM) 2.2 (Döll et al., 2003; Müller et al., 2014) with a spatial resolution of  $0.5^{\circ} \times 0.5^{\circ}$  and monthly steps were applied.
- (2) **GLDAS:** The averages of the four monthly land surface model simulations (i.e. CLM, Mosaic (MOS), VIC (Variable Infiltration Capacity) and NOAH with  $1^{\circ} \times 1^{\circ}$  grid from Global Land Data Assimilation System (GLDAS) data (Rodell et al., 2004) were used.
- (3) **CPC:** The Climate Prediction Center (CPC) has produced global  $0.5^{\circ} \times 0.5^{\circ}$  modeling datasets of monthly runoff, evapotranspiration, and soil moisture from 1948 until now, along with the consistent observation-based forcing datasets of precipitation and temperature (Dool et al., 2003). Monthly soil moisture data from CPC were used.

### 2.4. In Situ, HYDROWEB, CryoSat-2, ICESat and SRTM Data

- (1) **In Situ Data:** The Chenlingji and Hukou are the hydrological control stations of Doting and Poyang Lake, respectively (Figure 1a). The daily data from 2003 to 2016 of the TGR water level were obtained from <http://www.cjw.gov.cn/>.
- (2) **HYDROWEB Data:** Crétaux et al. (2011) provided a time series of global lake water levels by processing the data from the satellite altimetry missions Topex-Poseidon, GFO, ERS-2, Jason-1, Jason-2, and Envisat (<http://hydroweb.theia-land.fr/>).
- (3) **CryoSat-2:** Launched by the European Space Agency (ESA) in April 2010, it was the first

altimetry satellite equipped with a synthetic aperture radar altimeter that had the main task of monitoring changes in the polar ice sheet and ocean ice thickness to study the feedback mechanisms of climate and sea ice changes (Jiang et al., 2017). The L2 SARIN data were used to determine the GMC at the source of YRB-Geladandong. Due to the scarcity of the L2 SARIN data at Geladandong, the CryoSat-2 data were combined with the monthly resolution.

(4) **ICESat:** The ICESat mission was launched in January 2003 as part of the NASA Earth Observing System (EOS). The sole instrument onboard ICESat was the Geoscience Laser Altimeter System (GLAS), which was a laser altimeter and first provided a high-precision dataset (Cornelis, 2007). The GLA14 (Version 34) data were used (see Brenner et al., 2003; Surazakov et al., 2006).

(5) **SRTM:** The Shuttle Radar Terrestrial Mission (SRTM) used the interferometric synthetic aperture radar (InSAR) to measure the elevation within the latitudes  $\pm 60^\circ$  (Farr, 2007). The 3-arc-second gridded digital elevation model (DEM) of SRTM V4.1 (<http://srtm.csi.cgiar.org/srtmdata/>) was used as the reference elevation in this study to assist the GM changes at the Geladandong estimated from CryoSat-2/ICESat.

Detailed information on the datasets used is provided in Table 2.

### 3. Method

The TWS changes can be disintegrated into climate-driven changes, and human-induced changes (Reager et al., 2016). The climate-driven change includes the components of surface water storage (SWS), GMC, SM and GWS, while the human-induced change includes HGWS and reservoir impoundment (RI) (Syed et al., 2008; Reager et al., 2016). The SWS is the sum of the

LWS and RI, while the GWS is the sum of CGWS and HGWS:

$$\begin{aligned}
 TWS \text{ changes} &= \underbrace{LWS + SM + CGWS + GMC}_{\text{Climate-driven}} + \underbrace{HGWS + RI}_{\text{Human-driven}} \\
 SWS &= LWS + RI \\
 TGWS &= CGWS + HGWS
 \end{aligned} \tag{2}$$

The TWS change is inferred from the GRACE data. Precipitation (P), evapotranspiration (ET), and runoff (R) are used to verify GRACE-based TWS changes based on the water balance closure (Famiglietti et al., 2011; Long et al., 2014). The simulation data of the National Center for Atmospheric Research (NCAR) Community Land Model (NCAR-CLM4.0) (Bonan et al., 2011), WaterGAP Global Hydrology Model (WGHM) (Döll et al., 2003; Müller et al., 2014), Global Land Data Assimilation System (GLDAS) data (Rodell et al., 2004), and Climate Prediction Center (CPC) (Dool et al., 2003), were also used to compare with TWS change from GRACE data.

- (1) LWS (mainly from the Doting and Poyang Lake) (Schmidt et al., 2008) and RI (Three Gorges Reservoir impoundment (TGRI)) were validated by combining the remotely sensed lake level data from HYDROWEB (Crétaux et al., 2011), and in situ surface water level data.
- (2) SM was inferred from the GLDAS data.
- (3) TGWS was estimated by combining GRACE TWS data with simulated GLDAS data. Given that SWS in lakes, reservoirs, and river channels were not simulated in all the GLDAS models (Rodell et al., 2004). TGWS is estimated by subtracting the GRACE TWS by the simulated GLDAS LWS and the observed surface water of the TGRI.
- (4) CGSW was estimated from NCAR-CLM4.0 because it is the only model with the groundwater representation among all used models.

- (5) The human-induced TWS change in the TGR is estimated from the TWS difference between GRACE and NCAR-CLM4.0.
- (6) The HGWS is estimated from subtracting TGWS from the CGWS.
- (7) The CryoSat-2, ICESat and SRTM data were combined to monitor GMC at the Geladandong.

### 3.1. Lagrange multiplier method to minimize the leakage errors in GRACE data processing

Owing to the insufficient spatial resolution (300–400 km) of the GRACE mission, the determined TWS changes were spatially smoothed grids rather than point measurements. Wahr et al. (1998) proposed a simple Gaussian smoothing method (Jekeli, 1998), but this method was unable to isolate TWS changes in a specific region, such as YRB. Additional technology is required to estimate the basin TWS changes using GRACE data. The Lagrange multiplier method (LMM) was proposed to isolate the basin TWS changes in Swenson et al. (2002). The LMM is fixed to one type of error (satellite or leakage errors) to a specific value and minimizes the other type of error (leakage or satellite errors). This study employed the LMM with minimum signal leakage error to determine TWS changes in the YRB on the basis of the fixed satellite measurement error. Note that LMM was used in this study to estimate monthly TWS changes at a special basin rather than inferring any spatial distribution patterns of TWS changes. For more details on the Lagrange multiplier method, see Swenson et al. (2002) and Chao et al. (2017a).

In order to verify TWS changes, the time derivative ( $dS/dt$ ) was determined (Famiglietti et al., 2011; Long et al., 2014) using the following equations:

$$dS/dt = P - ET - R \quad (3)$$

$$\frac{dS}{dt} \approx \frac{dTWS}{dt} \approx \frac{TWS(t) - TWS(t-1)}{\Delta t} \quad (4)$$

As  $dS/dt$  estimated from GRACE via the central difference scheme in Eq.(4) above approximates the ‘true’ derivatives, and in order to be temporally consistent with TWS changes from GRACE data, Landerer et al. (2010) proposed smoothing the time series of the other water cycle variables according to

$$\tilde{F}_t = \frac{1}{4}F_{t-1} + \frac{1}{2}F_t + \frac{1}{4}F_{t+1} \quad (5)$$

where the F variables are the time series of P, ET, and R. The indices t-1, t, and t+1 refer to the previous, current, and following month, respectively.

Additionally, the original signal of TWS changes can be represented as the sum of long-term component, period and remaining residuals (Humphrey et al., 2016). The time series can be fitted by using the nonlinear least square method, including that the linear trend, interannual and semiannual cycle, and the remaining residuals. The time interval of TWS change is monthly, so a 13-month window moving average is a reasonable choice for estimating the long-term component (i.e., interannual and secular) (Humphrey et al., 2016).

### **3.2. Estimation of Glacier Mass Change (GMC) of Geladandong from the CryoSat-2/ICESat and SRTM Data**

The CryoSat-2/ICESat technique of precision spacecraft pointing control is not used over the rugged terrain such as QTP or in the mid-latitudes (59°S~59°N), so it is difficult to obtain reliable elevation changes using both the collinear method and the crossover method (Moholdt et al., 2010). Such difficulty can be mitigated by combining the ICESat elevation measurements with the SRTM-derived elevations (e.g., Käab et al., 2012; Gardner et al., 2013; Neckel et al., 2014). CryoSat-2/ICESat and DEM of SRTM were used to detect GMC at the Geladandong. Since the

technical details of this method can be found in Chao et al. (2017b), only a brief description is given in the following.

(1) Using the Landsat-7 images on July 10, 1999 (path 138 and row 37), and on June 3, 2000 (path 137 and row 37), a preliminary judgment of the ICESat footprints over the Geladandong glaciers was made by using the ratio of BAND3/BAND5  $\geq 2.2$ . Then, based on the Chinese Glacier Inventory (CGI) (Guo et al., 2015) and Google Earth images, the final CryoSat-2/ICESat footprints suitable for studying elevation changes over the Geladandong glaciers were determined.

(2) According to Nuth and Kääb (2011) and Gardelle et al. (2012), the elevations from the SRTM DEM cannot be directly used to determine the differenced elevation map with a CryoSat-2/ICESat-derived elevation. Therefore, corrections are required to determine the universal co-registration, elevation effect, and radar penetration effect.

(3) The heights from the CryoSat-2/ICESat are converted to the WGS84 system, and edited by using an empirical procedure to remove the outliers (Chao et al., 2017b).

(4) The median of the differences between the CryoSat-2/ICESat and SRTM elevations and their trends from the robust fitting are inferred.

### 3.3 Component contribution ratio

The component contribution ratio (CCR) (Kim et al., 2009) was used to quantify the mean percentage contribution of individual water storage components to the temporal variability of the original TWS estimates:

$$CCR_s = \frac{MAD_s}{TC} \quad (6)$$

where  $MAD_s = \frac{1}{N} \sum_S^{Storages} |S_t - \bar{S}|$ , which is the mean absolute deviation (MAD) of a storage

component;  $TC = \sum_S^{Storages} MAD_S$ , which is the TWS change (TC),  $S$  is the each component of TWS, such as GMC, SWS, SM and GWS.

### 3.4 Uncertainty Estimation

In this study, the TWS change from the LMM was used. The other eight TWS changes from different GRACE solutions were only used to cross-validate TWS change from LMM. Therefore, the uncertainty of TWS changes from LMM was only estimated as the sum of GRACE measurement errors and the (bias/leakage) correction errors, which have been provided in associated products. Uncertainty of P and ET estimates was calculated as the standard deviation from differences model data (Tiwari et al., 2009; Pan et al., 2017). Uncertainty for GMC from ICESat, CryoSat-2, and SRTM can be found in Chao et al. (2017b).

The uncertainty in the trend of each component TWS change was determined from GRACE measurement errors as well as the CLM4.0 and GLDAS model output errors (Joodaki et al., 2014). Assuming that there is no correlation between monthly GRACE data and their contribution to the uncertainty was estimated as the 2-sigma formal error of the trend. The trend of hydrology uncertainty in the YRB was estimated as the absolute value of the difference between CLM4.0 and GLDAS. Finally, the total uncertainty was obtained by adding in quadrature to the model and measurement uncertainty, as given in Table 3.

## 4. Results and Discussion

### 4.1. TWS changes in the YRB from GRACE data

The TWS changes in the YRB from LMM were verified from in situ data of P, ET, and R (Figure S1), other eight products of GRACE TWS, and four products of hydrological models

TWS (Figure S2). First, the different products of P and ET are compared with the in situ data from weather stations (Figure S1), and they were used to infer the water balance (P-ET-R) results (Figure 2).

From Figure S1, P and ET from different products are consistent with the in situ data, where the correlation coefficients (CC) are both over 0.9. However, the root mean square error (RMSE) of ET is larger than that of P.

Figures 2a–d show that the observed water balance agrees with the TWS changes observed from GRACE data, but they are also different, especially the amplitude. The main reasons may be ET, because ET data are difficult to estimate and have a large uncertainty (Figure 3b) (Long et al., 2014). The CC and RMSE between the LMM TWS and water balance TWS from Equation (3) are 0.70 and 2.69 cm respectively, but they can be improved to 0.80 and 1.48 cm when Equation (4) is used.

From Figure S2a–h, the TWS estimates from different GRACE data post-processing methods are generally consistent. The CC and RMSE of the TWS between the LMM and four DDK5 products were over 0.8, and approximately 1.80 cm, respectively, but the CC and RMSE of the Mascon TWS are over 0.9, and about 1.50 cm, respectively. The best TWS agreement with LMM is the JPL FAN product.

From Figure S2i–l, the CC and RMSE of the TWS between the LMM and four hydrological model products are nearly 0.74 and 2.24 cm, respectively, which are somewhat low. The GLDAS TWS exhibited the best performance. Although TWS changes from GRACE data can be seen as hydrological signals after deducing other signals (such as atmospheric and ocean) from the

background model, but they are different from those of the hydrological model. In addition, there are errors in the background and hydrological models, which can also cause differences. This indicates that TWS from hydrological models cannot be fully equal to GRACE TWS.

Figure 3 shows the annual change and seasonal cycle of the TWS, P, ET and R, which show that (1) the uncertainty of ET is larger than that of P and TWS, (2) the trend and annual variability of P, ET and R remain stable, but TWS increases, (3) the TWS changes, P, ET, and R in the YRB have obvious seasonal cycles with maxima in summer and minima in winter.

## **4.2. Individual components of TWS changes**

### **4.2.1. GMC at the Geladandong**

The GMC at the Geladandong was derived using the CryoSat-2, ICESat, and SRTM data during the period of 2003–2016, showing that GMC and its trends were all negative before and after the SRTM correction (Figure 4). The trend of the GMC was  $-0.158 \pm 0.066 \text{ m}\cdot\text{yr}^{-1}$  during 2003–2009 from the ICESat and SRTM data,  $-0.043 \pm 0.032 \text{ m}\cdot\text{yr}^{-1}$  during 2010–2016 from the CryoSat-2 and SRTM data, and  $-0.025 \pm 0.013 \text{ m}\cdot\text{yr}^{-1}$  by fitting the elevation difference between CryoSat-2/ICESat and SRTM data during 2003–2016. The annual variability of GMC at Geladandong also declined. These results show that the glaciers in this area were melted. The cause of the Geladandong glacier melt was investigated by Chao et al. (2017b) from the surrounding hydroclimatic data, showing that an increase in temperature leads to glacial melt. The contribution of GMC in Geladandong to the total TWS change (CCR) was 15%.

### **4.2.2. TGR and its impacts on the TWS changes**

TGR is the most important water control project in the world. The total length, crest height

and area are 3,035 m, 185 m, and 1,084 km<sup>2</sup>, respectively. The initial reservoir level and final reservoir level are 156 m and 175 m, respectively. The total impoundment capacity is 39.3 billion m<sup>3</sup>, and the flood control capacity is 22.15 billion m<sup>3</sup>. TGR construction began in 1994 and was completed in 2009. The first impoundment, up to 136 m, was in 2003. The first test and final impoundment of up to 175 m were in 2008 and 2010, respectively, and an impoundment of up to 175 m occurred between October and November. TGR impoundment is disintegrated into two phases, one with an impoundment level less than 175 m, and the other with an impoundment level of 175 m. More details of the TGRI can be seen in Figure 5a and Liu et al. (2016).

The region of 3°×3° around the TGR is used to infer the effect of water storage after impoundment. Because the impoundments of TGR are irregular, their influence on TWS changes cannot be modeled by the existing hydrological models but can be reflected in TWS changes from GRACE data. Hence, the difference in TWS changes between GRACE data and hydrological model can be considered human-induced. In the selected hydrological models, GLDAS data do not include groundwater, and the time span of the WGHM data was only 2002–2012. TWS changes from GRACE data subtract the sum of soil moisture, snow, canopy, river storage, and CGWS from CLM4.0 data as the human-induced TWS, which is a TWS change due to TGRI.

The human-induced TWS change in TGR (Figure 5c) was obtained by the total TWS change from GRACE (Figure 5b), subtracting the TWS change from NCAR-CLM4.0. Therefore, the human-induced TWS change could be obtained for each month with the same resolution of GRACE. During April 2002 to May 2003, TGR was not impoundment. The human-induced TWS change in the TGR from April 2002 to May 2003 could be taken as the other human effects (such

as irrigation), but during June 2003 to December 2015, there was impoundment in TGR, and the human-induced TWS change should be the sum of TGRI and other human effects. Therefore, the difference between the mean of human-induced TWS change from April 2002 to May 2003 and from June 2003 to December 2015 (Figure 5d) can be seen as the TGRI effect. The results of Figure 5d show that TGRI caused the water storage to increase around the TGR and decrease in the lower lakes. From Figures 5b–d, TGRI could lead to TWS changes, and the water storage in the YRB and TGR increased after impoundment.

Figures 7a and 7b show the annual variability and seasonal cycle in the water level changes of the TGR during 2003–2013. The results show that the water level change was minima in summer but maxima in November, and the annual variability increased, indicating that the water level change of the TGR was human-dominated.

#### **4.2.3. LWS from altimetry and in situ hydrological stations**

The Poyang and Doting lake water level changes were obtained from the HYDROWEB (Crétaux et al., 2011), and the surface water level data were obtained from Chenlingji and Hukou in situ hydrological stations (Figures 6a and 6b). The CC and RMSE between the surface water level from altimetry and in situ data in Poyang are 0.88 and 0.59 m, respectively, in Doting Lake are 0.60 and 0.67 m, respectively.

The LWS is the sum of Poyang Lake, Doting Lake and others lakes in the YRB. The results of other lakes and reservoirs are from Cai et al. (2016), who investigated the water storage dynamics of 128 large lakes and 108 reservoirs in the YRB.

From Figure 7a and 7b, the annual variability increased and the maxima in 2010 due to the

severe flood in the middle and lower YRB. The lake water level change showed a clear seasonal cycle with maxima in summer and minima in winter.

#### 4.2.4. Results from SWS, SM and GWS

SWS, SM, TGWS, HGWS, and CGWS were derived from the GRACE, GLDAS, and CLM4.0 data based on Equation (1). SWS is the sum of LWS and TGRI; SM is obtained from GLDAS; TGWS was obtained by taking the difference of the TWS changes from GRACE and GLDAS, Poyang Lake, Doting Lake and TGR water level change data. Hereafter, TGWS is represented by GRACE-GLDAS. The HGWS was obtained by taking the difference between the TWS changes from GRACE and CLM4.0 data. Hereafter, HGWS was represented by GRACE-CLM4.0. CGWS was obtained from CLM4.0 data. The trends of SWS, SM, TGWS, HGWS, and CGWS in YRB during 2003–2015 were  $0.56\pm 0.07$  Gt yr<sup>-1</sup>,  $1.65\pm 0.88$  Gt yr<sup>-1</sup>,  $10.39\pm 1.27$  Gt yr<sup>-1</sup>,  $4.87\pm 1.12$  Gt yr<sup>-1</sup> and  $5.52\pm 1.69$  Gt yr<sup>-1</sup>, respectively (Table 3). The contributions of SWS, SM, and GWS to TWS (CCRs) are 12%, 25% and 48% in the YRB, respectively.

The fitted from the nonlinear least square method and long-term component from 13-windows method of total TWS changes, HGWS and TGWS are shown in Figure S3. From Figure S3, the periods of TWS from the GRACE, CLM4.0, and GLDAS data agree with each other, and they show that changes in TWS and groundwater have increased since 2008. As shown in Figure 7a, the annual variability of SM was stable, but TGWS and HGWS obviously increased. In addition, the years 2006, 2010, and 2011 exhibited larger peaks associated with El Niño–La Niña events (Zhang et al., 2015). During El Niño years, the YRB receives more rainfall than

normal (Zhang et al., 2015). During la Niña years, the YRB is drier than that in normal years (Zhang et al., 2015). The droughts of 2006 and 2011 and the floods of 2010 (Zhang et al., 2015; Zhou et al., 2017) were also well captured. From Figure 7b, SM, TGWS and HGWS show a strong seasonal cycle with maxima in summer and minima in winter. The maximum seasonal cycle of TWS changes, SM, TGWS, and HGWS were 7.3 cm, 2.4cm, 3.8cm, and 3.3cm at July, respectively.

#### **4.3. Relationship between TWS change and each individual component**

From Table 4, the correlation coefficients between P and ET, ET and R, and R and P were approximately 0.7, with p-value less than 0.001, indicating that they are strongly related to each other. The maximum correlation between P, ET, R, and TWS was runoff, with a correlation coefficient of 0.71 with a p-value less than 0.001. The results of the correlation between SM and P, ET, R, TWS, GMC, TGR, Poyang Lake, Doting Lake, TGWS, and HGWS showed that SM is mainly influenced by river runoff in the YRB. The correlation coefficient between the GMC at the Geladandong and TWS shows a moderate correlation, indicating that the glacier melt has a certain effect on the TWS changes in the YRB.

There is a strong relationship between P, ET, and R, and lakes (Poyang Lake and Doting Lake). There was no correlation between P, ET, R, and TGR, and TGR and lakes (Poyang Lake and Doting Lake), indicating that the TGR does not affect the lake water changes, and the lake water changes are mainly due to climate change. This result is coincide with that of Wang et al. (2017), who found that climate variability is the dominant driver of the recent decadal lake decline across China's Yangtze Plain.

The results of the correlation coefficient between TWS and TGWS, HGWS indicate that the increase in TWS is mainly from GWS. The TGR, TGWS, and HGWS also have a strong correlation, indicating that the TGR has a certain contribution to the increase in GWS, but more data (e.g., well data) are required for further investigation.

The GRACE data over 13 years (2003–2015) showed that the trends of TWS changes and TGWS were  $12.04 \pm 1.81 \text{ Gt yr}^{-1}$  and  $10.39 \pm 1.27 \text{ Gt yr}^{-1}$ , respectively, accounting for 86% of TWS changes. Because the well data in the YRB is coarse, hard to obtain, and cannot be found in the literature, the above conclusions are not verified. The groundwater changes estimation method used is the same as reported by Joodaki et al. (2014), who verified groundwater changes in the Middle East by using well data in Iran. Moreover, GRACE and model data can jointly provide another effective method for understanding hydrological processes in the area of sparse data.

The increase in TWS changes in the YRB mainly from groundwater during 2003–2015 and the spatial distribution of the sum of TGWS and SWS (TGSW) trend were obtained by subtracting GLDAS data from GRACE data for 2003–2015 (Figure 8). The method to infer the spatial map of the TGSW trend can be seen in Joodaki et al. (2014). As shown in Figure 8, TGSW increased around the TGR and the headwaters of the Yangtze River, but TGWS decreased in the lower sub-basin, such as Tai Lake. From the spatial distribution of the TGSW trend over the YRB, TGSW was observed to increase. Due to the limitations of the low temporal-spatial resolution of GRACE data and the shortage of in situ data, it is difficult to determine the causes of TGSW increase, such as whether TGR impoundment can increase TGSW in the YRB. To investigate the cause of this increase, in situ data (such as well data around the TGR) should also be used.

## 5. Conclusions

TWS changes in the YRB were inferred using LMM from 13 years of GRACE data during the period of 2003–2015. The components of TWS variability were also investigated by disintegrating TWS changes into individual components (such as glacier, soil moisture, surface water, and groundwater). The GMC at the Geladandong can be detected by using the CryoSat-2, ICESat and SRTM data. Groundwater can be effectively monitored using GRACE, altimetry and hydrological data. The main findings are as follows:

- (1) TWS changes in the YRB can be effectively inferred using LMM from GRACE data, and the trend of TWS change was  $12.04 \pm 1.81 \text{ Gt yr}^{-1}$  during 2003–2015.
- (2) The glaciers at the Geladandong were melted during 2003–2016 from CryoSat-2, ICESat, and SRTM data.
- (3) The trend of TGRI accounts for ~3% of the trend in TWS variability in the YRB during the period 2003–2015, indicating that TGRI has a moderate effect on the TWS changes in the YRB, leading to an TWS increase in TWS in the YRB.
- (4) The trend of surface water storage anomalies (including GMC at the Geladandong, Three Gorges Reservoir impoundment, and storage change in the Lakes Doting and Poyang) account for only ~6% of the trend in TWS variability over the YRB.
- (5) TWS changes, soil moisture storage anomalies, lake water changes and GWS anomalies show a clear seasonal cycle with maxima in summer and minima in winter, but the water changes of TGR are minima in summer and maxima in November due to impoundment. The annual variability of the TWS components is increasing except for Geladandong glaciers.

(6) The increased groundwater storage in the YRB has a large effect on TWS changes.

In this study, we investigate the component contributions to the spatiotemporal variability of total TWS in the YRB, which provides new valuable insights for understanding the distribution of water resources. The method discussed in this paper can be applied to other river basins all over the world. Therefore, the water resource distribution of each river basin in the world will be derived, which can provide information for the basis of constructive suggestions for water resource management.

With the development of satellite technology, such as ICESat-2 (Abdalati et al., 2010, it was launched on 15 September 2018) and GRACE Follow-On mission (Flechtner et al., 2014, it was launched on 22 May 2018), satellite observations will be better utilized to investigate water storages and their contribution to global sea level rise. Quantitative estimation of the hydrological elements for each of the global river basins using multisource satellite observations is crucial to understand global sea level rise.

**Acknowledgments:** The authors thank the following data providers for making the data available: GRACE-CSR, JPL, GFZ, GRGS; Altimetry; SRTM; GLDAS; CPC; WGHM; runoff; in situ water level; TRMM; GPCP, National Meteorological Information Center and CLM4.0 from Prof. Lo Minhui. This study is supported by the NSFC (China) under Grants 41974019, 41704011, 41721003, and 41974007; Supported by the CRSRI Open Research Program (Program SN: CKWV2019728/KY), and Natural Science Foundation of Hubei Province of China under Grant 2019CFB427.

## References

- A, G., Wahr, J., Zhong, S. (2013), Computations of the viscoelastic response of a 3-D compressible Earth to surface loading: an application to glacial isostatic adjustment in Antarctica and Canada, *Geophys. J. Int.*, 192, 2, 557–572. <https://doi.org/10.1093/gji/ggs030>.
- Abdalati, W., Zwally, H.J., Bindschadler, R., Csatho, B., Farrell, S.L., Fricker, H.A., et al. (2010), The ICESat-2 laser altimetry mission, *Proc. IEEE.*, 98, 5, 735-751. [10.1109/JPROC.2009.2034765](https://doi.org/10.1109/JPROC.2009.2034765).
- Adler, R.F., Huffman, G. J., Chang, A., Ferraro, R., Xie, P., Janowiak, J., et al. (2003), The Version-2 Global Precipitation Climatology Project (GPCP) Monthly Precipitation Analysis (1979–Present), *J. Hydrometeorol.*, 4, 6, 1147–1167. [https://doi.org/10.1175/1525-7541\(2003\)004<1147:TVGPCP>2.0.CO;2](https://doi.org/10.1175/1525-7541(2003)004<1147:TVGPCP>2.0.CO;2).
- Anyah, R.O., Forootan, E., Awange, J.L., Khaki, M. (2018), Understanding linkages between global climate indices and terrestrial water storage changes over Africa using GRACE products, *Sci. Total Environ.*, 635, 1405–1416. <https://doi.org/10.1016/j.scitotenv.2018.04.159>.
- Bonan, G.B., Lawrence, P.J., Oleson, K.W., Levis, S., Jung, M., Reichstein, M., et al. (2011), Improving canopy processes in the Community Land Model version 4 (CLM4) using global flux fields empirically inferred from FLUXNET data, *J. Geophys. Res.*, 116, G02014, <http://dx.doi.org/10.1029/2010JG001593>.
- Brenner, A.C., Bentley, C.R., Csatho, B.M., Harding D.J., Hofton M.A., Minster J., et al. (2003), Derivation of Range and Range Distributions From Laser Pulse Waveform Analysis for

Surface Elevations, Roughness, Slope, and Vegetation Heights, *Algorithm Theoretical Basis*

*Document. Greenbelt. MD: Goddard Space Flight Center. Version 3.0.*

<http://citeseerx.ist.psu.edu/viewdoc/summary?doi=10.1.1.557.7523>.

Cai, X.B., Feng, L., Hou, X.J., Chen, Xiao.L. (2016), Remote Sensing of the Water Storage

Dynamics of Large Lakes and Reservoirs in the Yangtze River Basin from 2000 to 2014,

*Scientific Reports*, 6, 36405, 10.1038/srep36405.

Chao, N., Wang, Z. (2017a), Characterized flood potential in the Yangtze River basin from

GRACE gravity observation, hydrological model and in-situ hydrological station, *J. Hydrol.*

*Eng.*, [http://dx.doi.org/10.1061/\(ASCE\)HE.1943-5584.0001547](http://dx.doi.org/10.1061/(ASCE)HE.1943-5584.0001547).

Chao, N., Wang, Z., Hwang, C., Jin, T., and Cheng, Y. (2017b), Glacier retreat in Yangtze River's

source region detected by ICESat altimetry and assessed by hydroclimatic data, *Remote Sens.*

9, 1, Art. 75. <http://dx.doi.org/10.3390/rs9010075>.

Chen, J. (2020a). Hot issues of the Yangtze River. Evolution and Water Resources Utilization of

the Yangtze River. *Springer Singapore*, Singapore, pp. 1–45.

[https://doi.org/10.1007/978-981-13-7872-0\\_1](https://doi.org/10.1007/978-981-13-7872-0_1).

Chen, J. (2020b). Hydrological characteristics of the Yangtze River. Evolution and Water

Resources Utilization of the Yangtze River. *Springer Singapore*, Singapore, pp. 123–162.

[https://doi.org/10.1007/978-981-13-7872-0\\_3](https://doi.org/10.1007/978-981-13-7872-0_3).

Cheng, M., Ries, J., Tapley, B. (2011), Variations of the Earth's Fig. Axis from Satellite Laser

Ranging and GRACE, *J. Geophys. Res.*, 116, B01409,

<http://dx.doi.org/10.1029/2010JB000850>.

- Cornelis, S. (2007), Towards a combined estimation of Greenland's ice sheet mass balance using GRACE and ICESat data, *Holland: Delft University of Technology*, <https://doi.org/uuid:0d315b1b-84a4-4e03-8b65-95353e04a598?collection=education>.
- Crétaux, J.F., Jelinski, W., Calmant, S., Kouraev, A., Vuglinski, V., Berge-Nguyen, M., et al. (2011), SOLS: A lake database to monitor in the Near Real Time water level and storage variations from remote sensing data, *Adv. Space Res.*, 47, 9, 1497–1507. <https://doi.org/10.1016/j.asr.2011.01.004>.
- Döll, P., Kaspar, F., Lehner, B. (2003), A global hydrological model for deriving water availability indicators: Model tuning and validation, *J. Hydrol.*, 207, 1-2, 105–134. [http://dx.doi.org/10.1016/S0022-1694\(02\)00283-4](http://dx.doi.org/10.1016/S0022-1694(02)00283-4).
- Dool, H.V.D., Huang, H.J., and Fan, Y. (2003), Performance and analysis of the constructed analogue method applied to US soil moisture applied over 1981-2001, *Geophys. Res. Lett.*, 108, D16, 8617, <http://dx.doi.org/10.1029/2002JD003114>.
- Famiglietti, J.S., Lo, M.H., Ho, S.L., Bethune, J., Anderson, K.J., Syed, T.H., et al. (2011), Satellites measure recent rates of groundwater depletion in California's Central Valley, *Geophys. Res. Lett.*, 38, L03403, <http://dx.doi.org/10.1029/2010GL046442>.
- Farr, T.G., Rosen, P.A., Caro, E., Crippen, R., Duren, R., Hensley, S., Kobrick, M., Paller, M., Rodriguez, E., Roth, L., Seal, D. (2007). The shuttle radar topography mission. *Rev. Geophys.*, 45(2).
- Ferreira, V.G., Gong, Z., He, X., Zhang, Y., Andam - Akorful, S.A. (2013), Estimating Total Discharge in the Yangtze River Basin Using Satellite-Based Observations, *Remote Sens.* 5,

3415-3430.

Ferreira, V.G., Yong, B., Tourian, M.J., et al. (2020). Characterization of the hydro-geological regime of Yangtze River basin using remotely-sensed and modeled products. *Sci. Total Environ.*, 718, 137354

Flechtner, F., Morton, P., Watkins, M., & Webb, F. (2014), Status of the GRACE follow-on mission. IAG symposium gravity, geoid, and height systems, 141, 117–121.  
[https://doi.org/10.1007/978-3-319-10837-7\\_15](https://doi.org/10.1007/978-3-319-10837-7_15).

Gardelle, J., Berthier, E., Arnaud, Y. (2012). Impact of resolution and radar penetration on glacier elevation changes computed from multi-temporal DEMs. *J. Glaciol.*, 58, 419–422.

Gardner, A.S., Moholdt, G., Cogley, J.G., Wouters, B., Arendt, A.A., Wahr, J. (2013), A reconciled estimate of glacier contributions to sea level rise: 2003 to 2009, *Science* 340, 852–857. <http://dx.doi.org/10.1126/science.1234532>.

Guo, W., Liu, S., Xu, J., Wu, L., Shanguan, D., Yao, X., et al. (2015), The second Chinese glacier inventory: Data, methods and results. *J. Glaciol.*, 61, 226, 357–372.  
<http://doi.org/10.3189/2015JoG14J209>.

Hasan, E., and Tarhule, A. (2020). GRACE: Gravity Recovery and Climate Experiment long-term trend investigation over the Nile River Basin: Spatial variability drivers. *J. Hydrol.*, 586, 124870. <https://doi.org/10.1016/j.jhydrol.2020.124870>.

Heiskanen, W.A, Moritz H. (1967), Physical Geodesy. Freeman W H and Company, San Francisco, California and London, U K.

Huang, Q., Sun, Z.D., Opp, C., et al. (2014), Hydrological drought at dongting lake: its detection, characterization, and challenges associated with three gorges dam in central Yangtze, China. *Water Resour. Manag.*, 28, 15, 5377-5388.

- Huang, Y., M. S. Salama, M. S. Krol, Z. Su, A. Y. Hoekstra, Y. Zeng, and Y. Zhou (2015), Estimation of human induced changes in terrestrial water storage through integration of GRACE satellite detection and hydrological modeling: A case study of the Yangtze River basin, *Water Resour. Res.*, *51*, 8494–8516, doi:10.1002/2015WR016923.
- Huffman, G.J., Adler, R.F., Bolvin, D.T., Gu, G., Nelkin, E.J., Bowman, K.P. (2007), The TRMM Multi-satellite Precipitation Analysis: Quasi-Global, Multi-Year, Combined-Sensor Precipitation Estimates at Fine Scale, *J. Hydrometeor.*, *8*, 38-55. <https://doi.org/10.1175/JHM560.1>.
- Humphrey, V., Gudmundsson, L. & Seneviratne, S.I., (2016), Assessing global water storage variability from GRACE: trends, seasonal cycle, subseasonal anomalies and extremes, *Surv Geophys.*, *37*, 357. <https://doi.org/10.1007/s10712-016-9367-1>.
- Jekeli C. (1981) Alternative methods to smooth the earth's gravity field, *Rep.*, *327*, Department of Geodetic Science and Surveying, Ohio State University, Columbus.
- Jiang L., Nielsen K., Andersen, O. B., Peter B.G. (2017), Monitoring recent lake level variations on the Tibetan Plateau using CryoSat-2 SARIn mode data, *J. Hydrol.*, *544*, 109–124. <http://dx.doi.org/10.1016/j.jhydrol.2016.11.024>.
- Jiang, Q., Vagner G.F., Chen, J.S. (2016), Monitoring groundwater changes in the Yangtze River basin using satellite and model data, *Arab J Geosci.*, *9*, 500, DOI 10.1007/s12517-016-2522-7
- Joodaki, G., Wahr, J., Swenson, S. (2014), Estimating the human contribution to groundwater depletion in the Middle East, from GRACE data, land surface models, and well observations,

*Water Resour. Res.*, 50, 3, 2679–2692. <http://dx.doi.org/10.1002/2013WR014633>.

Kääb, A., Berthier, E., Nuth, C., Gardelle, J., Arnaud, Y. (2012). Contrasting patterns of early 21st century glacier mass change in the Himalayas. *Nature*, 488, 495–498.

Kim, H., Yeh, P., J.-F., Oki, T., Kanae, S. (2009), Role of rivers in the seasonal variations of terrestrial water storage over global basins, *Geophys. Res. Lett.* 36, L17402. <http://dx.doi.org/10.1029/2009GL039006>.

Kusche, J., Schmidt, Petrovic, S., Rietbroek R. (2009), Decorrelated GRACE time-variable gravity solutions by GFZ, and their validation using a hydrological model, *J. Geo.*, 83, 10, 903-913. <http://dx.doi.org/10.1007/s00190-009-0308-3>.

Landerer, F. W., J. O. Dickey, and A. Güntner. (2010), Terrestrial water budget of the Eurasian pan-Arctic from GRACE satellite measurements during 2003–2009. *J. Geophys. Res.*, 115, D23115, doi:10.1029/2010JD014584.

Long, D., Longuevergne, L., Scanlon, B.R. (2014), Uncertainty in evapotranspiration from land surface modeling, remote sensing, and GRACE satellites, *Water Resour. Res.*, 50, 2, 1131–1151. <http://dx.doi.org/10.1002/2013WR014581>.

Long, D., Y. Yang, Y. Wada, Y. Hong, W. Liang, Y. Chen, B. Yong, A. Hou, J. Wei, and L. Chen (2015), Deriving scaling factors using a global hydrological model to restore GRACE total water storage changes for China's Yangtze River Basin, *Remote Sens. Environ.*, 168, 177-193, doi:10.1016/j.rse.2015.07.003.

Luthcke, S. B. et al. (2013), Antarctica, Greenland and Gulf of Alaska land ice evolution from an iterated GRACE global mascon solution, *J. Glaciol.*, 59, 613–631.

- Moholdt, G., Nuth, C., Hagen, J., Kohler, J. (2010). Recent elevation changes of Svalbard glaciers derived from ICESat laser altimetry. *Remote Sens. Environ.* 114, 2756–2767.
- Mu, Q., Heinsch, F.A.; Zhao, M.; Running, S.W. (2007), Development of a global evapotranspiration algorithm based on MODIS and global meteorology data, *Remote Sens. Environ.*, 111, 519–536.
- Müller, S.H., Eisner, S., Franz, D., Wattenbach, M., Portmann, F.T., et al. (2014), Sensitivity of simulated global-scale freshwater fluxes and storages to input data, hydrological model structure, human water use and calibration, *Hydrol. Earth Syst. Sc.*, 18, 3511–3538.  
<https://doi.org/10.5194/hess-18-3511-2014>.
- Neckel, N., Kropáček, J., Bolch, T., and Hochschild, V. (2014), Glacier mass changes on the Tibetan Plateau 2003–2009 derived from ICESat laser altimetry measurements, *Environ. Res. Lett.* 9, 014009. <http://dx.doi.org/10.1088/1748-9326/9/1/014009>.
- Nuth, C., Kääb, A. (2011). Co-registration and bias corrections of satellite elevation data sets for quantifying glacier thickness change. *Cryosphere*, 5, 271–290.
- Pan, Y., C. Zhang, H. Gong, P. J.-F. Yeh, Y. Shen, Y. Guo, Z. Huang, and X. Li (2017), Detection of human-induced evapotranspiration using GRACE satellite observations in the Haihe River basin of China, *Geophys. Res. Lett.*, 44, 190–199, doi: 10.1002/2016GL071287.
- Peltier W.R., Argus D.F., Drummond R. (2015), Space geodesy constrains ice age terminal deglaciation: The global ICE-6G\_C (VM5a) model, *J. Geophys. Res. Solid Earth*, 120, 1, 450–487. <http://dx.doi.org/10.1002/2014JB011176>.
- Ramillien, G., Bouhours, S., Lombard, A., Cazenave, A., Flechtner, F., Schmidt, R., et al. (2008),

- Land water storage contribution to sea level from GRACE geoid data over 2003-2006, *Global. Planet. Change*, 60, 3, 381–392. <http://dx.doi.org/10.1016/j.gloplacha.2007.04.002>.
- Reager, J.T., Gardner, A.S., Famiglietti, J.S., Wiese, D.N., Eicker, A., Lo, M.H. (2016), A decade of sea level rise slowed by climate-driven hydrology, *Science*, 351, 6274, 699–703. <http://dx.doi.org/10.1126/science.aad8386>.
- Rodell, M., Famiglietti, J.S., Chen, J., Seneviratne, S.I., Viterbo, P., Holl, S., et al. (2004), Basin scale estimates of evapotranspiration using GRACE and other observations, *Geophys. Res. Lett.*, 31, L20504. <https://doi.org/10.1029/2004GL020873>.
- Save, H.S. (2020). "CSR GRACE and GRACE-FO RL06 Mascon Solutions v02", doi: 10.15781/cgq9-nh24.
- Scanlon, B.R., Zhang, Z.Z., Save, H., et al. (2018), Global models underestimate large decadal declining and rising water storage trends relative to GRACE satellite data, *Proc. Natl Acad. Sci. USA* 115, E1080–E1089.
- Schmidt, R., Flechtner, F., Meyer, U., Neumayer, K. H., Dahle, C., König, R., et al. (2008), Hydrological Signals Observed by the GRACE Satellites, *Surv. Geophys.* 29, 4-5, 319–334. <https://doi.org/10.1007/s10712-008-9033-3>.
- Sun, Z., Zhu, X., Pan, Y., Zhang, J. (2017), Assessing Terrestrial Water Storage and Flood Potential Using GRACE Data in the Yangtze River Basin, China, *Remote Sens.* 9, 1011.
- Sun, Z., Zhu, X., Pan, Y., Zhang, J., Liu, X., (2018), Drought evaluation using the GRACE terrestrial water storage deficit over the Yangtze River Basin, China, *Sci Total Environ.*, 634, 727-738. doi: 10.1016/j.scitotenv.2018.03.292.

- Surazakov, A.B., Aizen, V.B. (2006), Estimating volume change of mountain glaciers using SRTM and map-based topographic data, *IEEE Trans. Geosci. Remote Sens.*, 44, 2991–2995.  
<https://doi.org/10.1109/TGRS.2006.875357>.
- Swenson, S.C., Chambers, D.P., Wahr, J. (2008). Estimating geocenter variations from a combination of GRACE and ocean model output, *J. Geophys. Res.*, 113, B08410.
- Swenson, S.C., Wahr, J. (2002), Methods for inferring regional surface mass anomalies from Gravity Recovery and Climate Experiment (GRACE) measurements of time-variable gravity, *J. Geophys. Res.*, 107, B9, 2193.
- Syed T.H., Famiglietti J. S., Chambers D. P., Willis J. K., Hilburn K. (2008), Satellite-based global ocean mass balance estimates of inter annual variability and emerging trends in continental freshwater discharge, *Proc. Natl. Acad. Sci.* 107, 17916–17921.
- Tapley, B.D., Bettadpur, S., Watkins, M., Reigber, C. (2004), The gravity recovery and climate experiment mission overview and early results, *Geophys. Res. Lett.*, 31, 9, L09607.  
<https://doi.org/10.1029/2004GL019920>.
- Tiwari, V.M., Wahr, J., Swenson, S. (2009). Dwindling groundwater resources in northern India, from satellite gravity observations. *Geophys. Res. Lett.* 36 (18).
- Wahr, J., Molenaar, M., Bryan, F. (1998), Time variability of the Earth's gravity field: hydrological and oceanic effects and their possible detection using GRACE, *J. Geophys. Res.*, 103, 30205–30229. <https://doi.org/10.1029/98JB02844>.
- Wang, J., Y. Sheng, and Y. Wada (2017), Little impact of the Three Gorges Dam on recent decadal lake decline across China's Yangtze Plain, *Water Resour. Res.*, 53, 3854–3877,

doi:10.1002/2016WR019817.

Watkins, M. M., Wiese D. N., Yuan D.-N., Boening C., Landerer F. W. (2015), Improved methods for observing Earth's time variable mass distribution with GRACE using spherical cap mascons, *J. Geophys. Res. Solid Earth* 120, 2648–2671. <https://doi.org/10.1002/2014JB011547>.

Wiese, D.N., Yuan, D.N., Boening, C., Landerer, F.W., Watkins., M.M. (2018). JPL GRACE Mascon Ocean, Ice, and Hydrology Equivalent Water Height Release 06 Coastal Resolution Improvement (CRI) Filtered Version 1.0. Ver. 1.0. PO.DAAC, CA, USA. Dataset accessed [YYYY-MM-DD] at <http://dx.doi.org/10.5067/TEMSC-3MJC6>.

Yin, H., Li, C. (2001), Human impact on floods and flood disasters on the Yangtze River, *Geomorphology*, 41, 2-3, 105-109.

Zhang, B., Zhang, E.Z., Liu, L., et al. (2018a), Geodetic measurements reveal short-term changes of glacial mass near Jakobshavn Isbrae (Greenland) from 2007 to 2017, *Earth Planeth Sc. Lett.*, 503, 216-226, doi: 10.1016/j.epsl.2018.09.029.

Zhang, D., Liu, X., Bai, P. (2019), Assessment of hydrological drought and its recovery time for eight tributaries of the Yangtze River (China) based on downscaled GRACE data, *J. Hydrol.*, doi: <https://doi.org/10.1016/j.jhydrol.2018.11.030>.

Zhang, D., Zhang., Q., Qiu, J.M., Bai, P., et al. (2018b), Intensification of hydrological drought due to human activity in the middle reaches of the Yangtze River, China, *Sci Total Environ*, 637, 1432-1442.

Zhang, Z., Chao, B.F., Chen, J., Wilson, C.R. (2015), Terrestrial water storage anomalies of

Yangtze River Basin droughts observed by GRACE and connections with ENSO, *Glob.*

*Planet Chang.* 126, 35–45.

Zhang, Z.Z., Chao, B.F., Lu, Yang., Hsu, H.T. (2009), An effective filtering for GRACE time-variable gravity: fan filter, *J. Geophys. Res.*, 36, L17311.

Zhou, H., Luo, Z., Tangdamrongsub, N., Wang, L., He, L., Xu, C., Li, Q. (2017), Characterizing Drought and Flood Events over the Yangtze River Basin Using the HUST-Grace2016 Solution and Ancillary Data, *Remote Sens.*, 9, 1100.

**Conflicts of Interest:** The authors declare no conflict of interest.

Nengfang Chao and Taoyong Jin: Conceptualization and Methodology. Nengfang Chao, Taoyong Jin, Gang Chen, Xianglin Liu, Zhengtao Wang: Data curation, Writing, Original draft preparation. Zuansi Cai, Gang Chen, Xianglin Liu, Zhengtao Wang: Supervision. Nengfang Chao, Taoyong Jin, Zuansi Cai, Xianglin Liu: Writing, Reviewing and Editing.

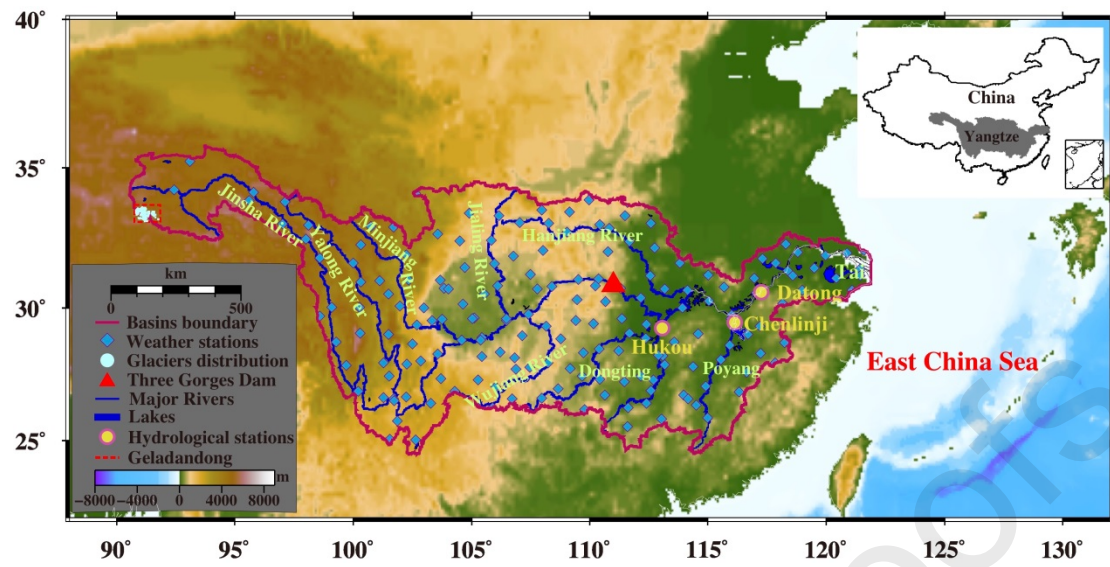


**Figure 1.** Study area. Major rivers, glacier distribution of the Geladandong area from the Chinese Glacier Inventory (Guo et al., 2015), weather stations and hydrological stations.

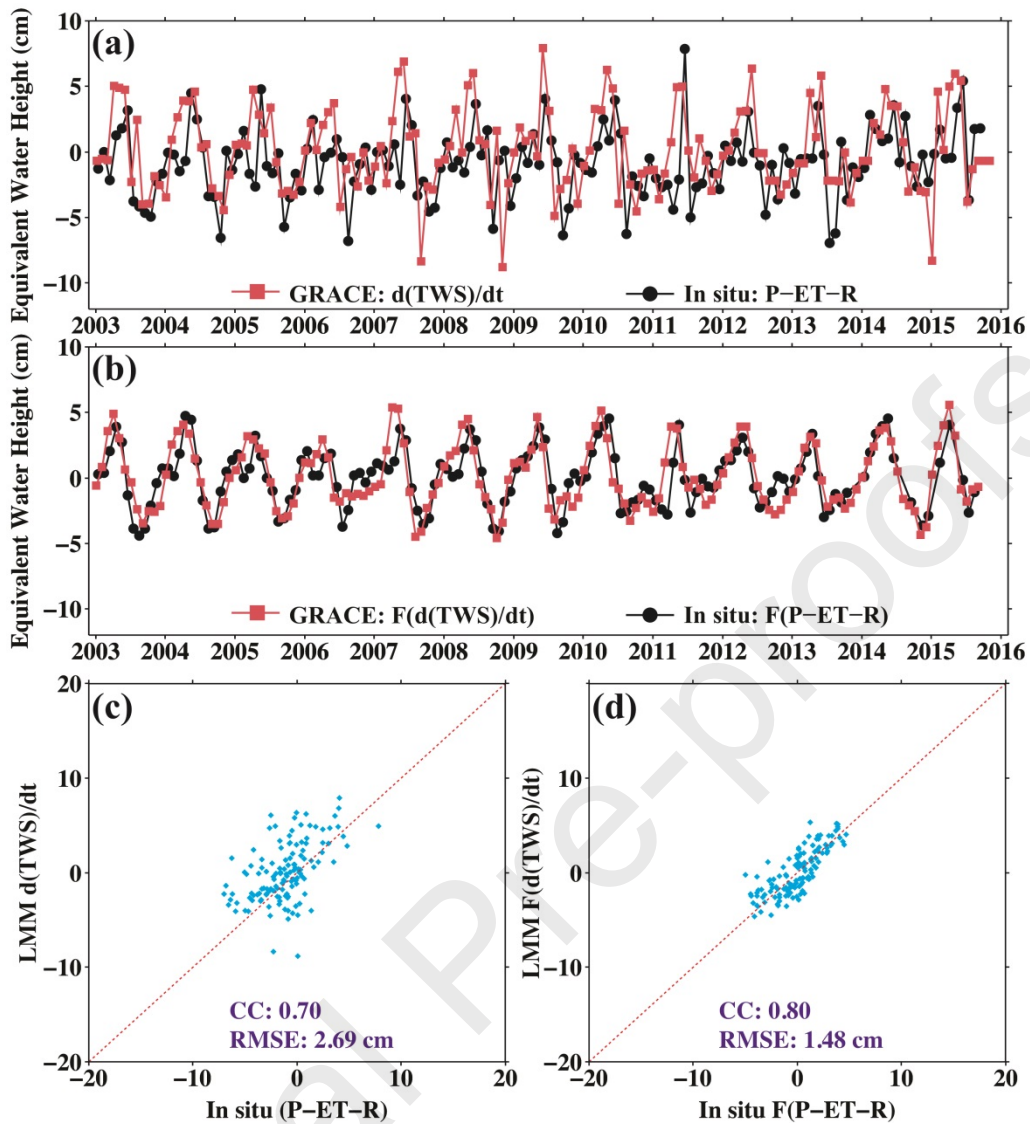


**Figure 2.** Comparison between TWS changes from LMM-GRACE and in situ data (a) basing on the Eq. (2) and (3), (b) basing on the Eq. (4). Scatterplots comparing (c) in situ data (P-ET-R) with LMM  $d(TWS)/dt$  and (d) in situ filter (P-ET-R) with LMM filter ( $d(TWS)/dt$ ). CC is correlation coefficient, and RMSE is root mean square error.

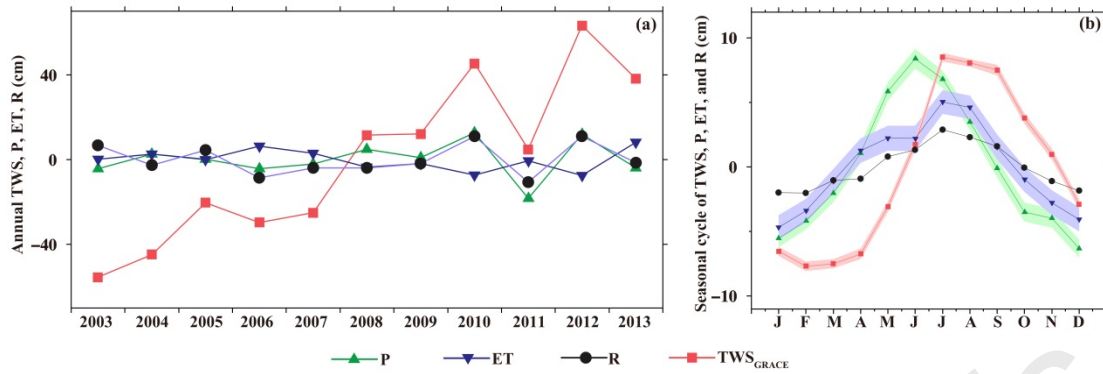


**Figure 3.** (a) Annual changes and (b) seasonal cycles of TWS, P, ET, and R. The pink and gray envelopes denote the uncertainties (i.e., errors) of GRACE, while the blue and green band denotes the uncertainty of P, ET estimates calculated as the standard deviation from differences models data (see Section 3.4 for details).

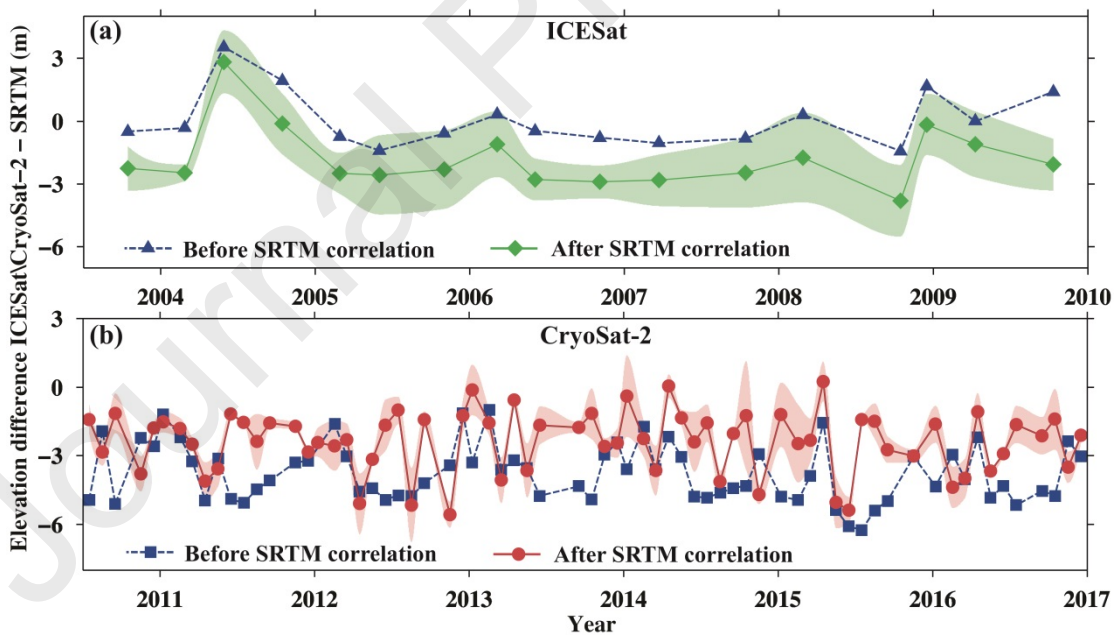


**Figure 4.** Glacier elevation changes are determined by using all median values of the elevation differences between (a) ICESat, (b) CryoSat-2 and SRTM data during 2003–2016. The shaded envelopes represent the corresponding uncertainties (see Chao et al. (2017b) for details).

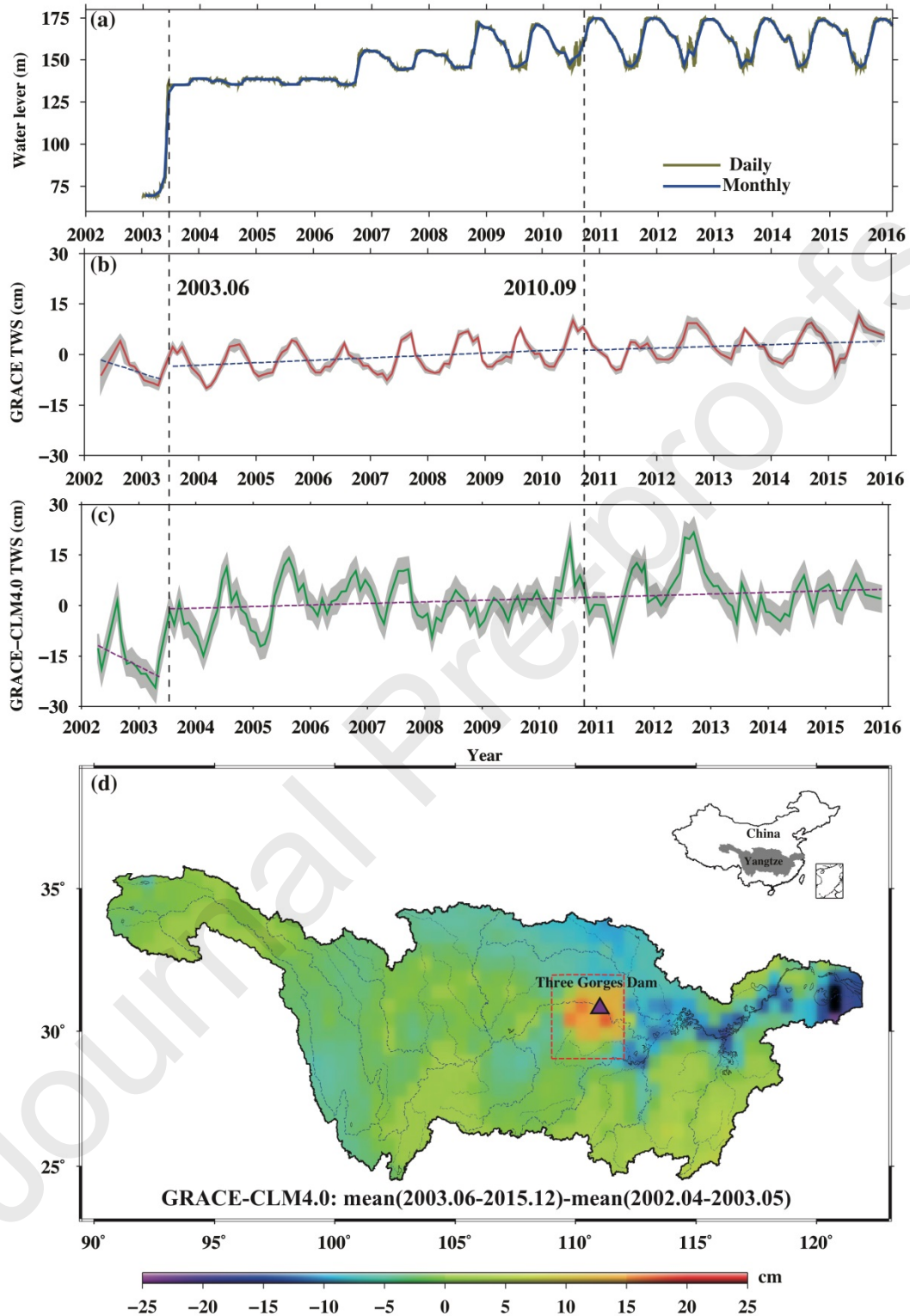


**Figure 5.** (a) Water level changes of TGR during 2003–2016 from in situ data. (b) Time series of TWS changes in the TGR (3° × 3°) before and after impoundment from the GRACE data. (c) The

human-induced TWS changes in the TGR from the GRACE-CLM4.0. (d) The differences in TWS changes between the mean of June 2003–Dec 2015 and Apr 2002–May 2003 after GRACE-CLM4.0. The shaded envelopes in (b) and (c) represent the corresponding uncertainties (see Section 3.4 for details).

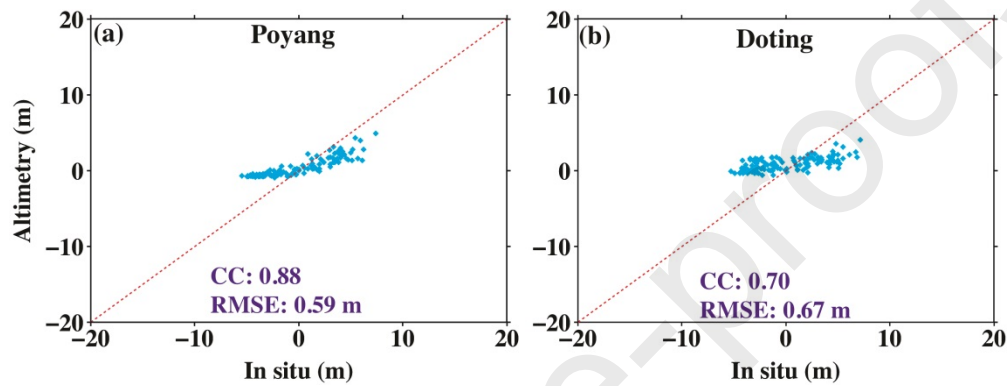


**Figure 6.** Scatterplots comparing surface water level change from altimetry with in situ data at (a) Poyang Lake from the Chenlingji station, and (b) Doting Lake from the Hukou station.

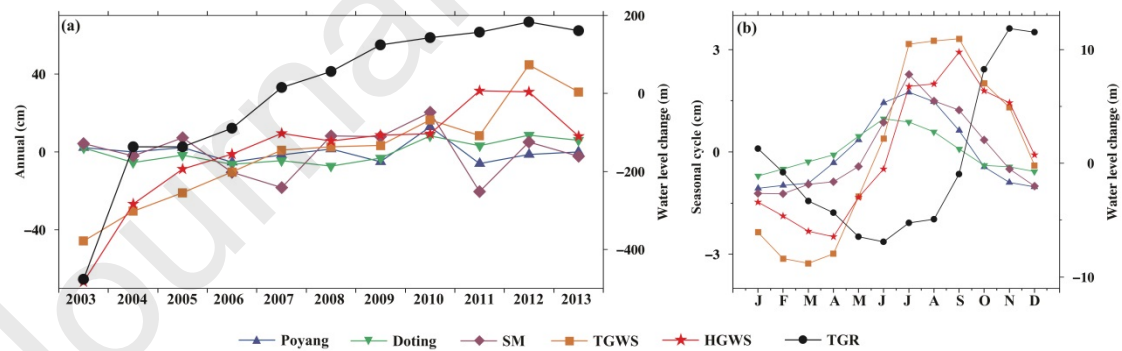


**Figure 7.** (a) Annual changes and (b) seasonal cycles of the Poyang Lake, Doting Lake, SM, TGWS, HGWS, and TGR surface water level.

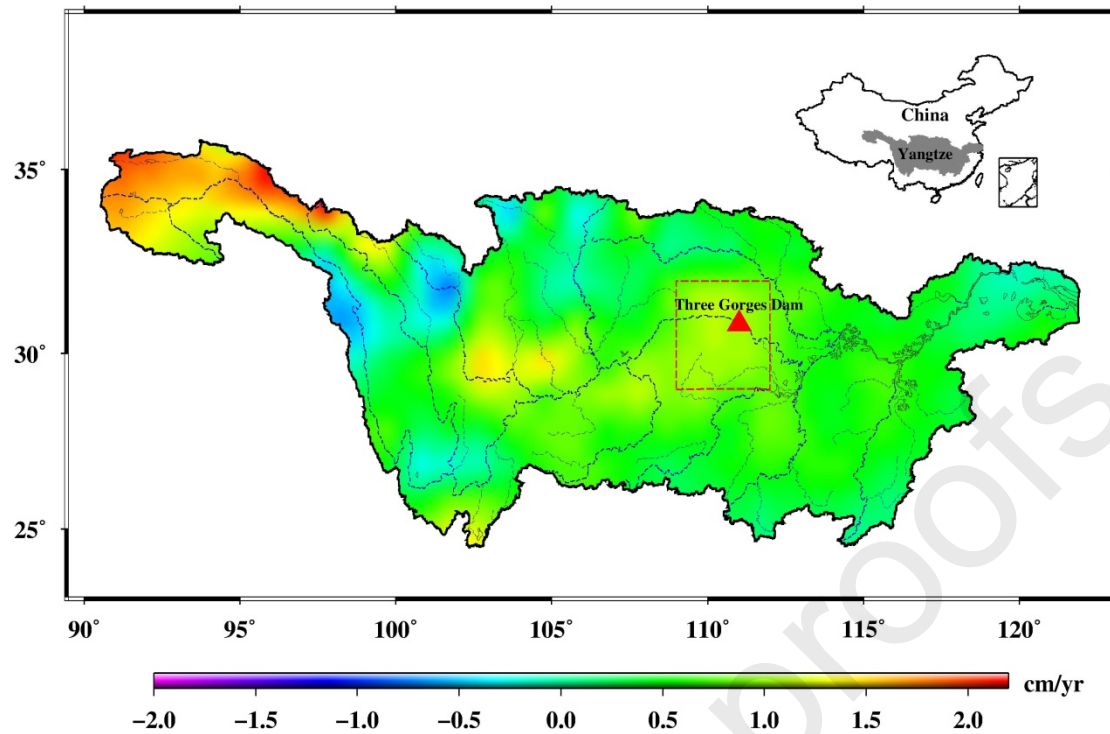


**Figure 8.** Spatial distribution trend with the sum of total groundwater storage anomaly (TGWS) and surface water storage anomaly (SWS) in the YRB during 2003–2015 from GRACE-GLDAS.

**Table 1**

Review of recent studies on the Yangtze River basin using GRACE data.

Referenc es	Focused	Source data	Main contributions
He et al., 2018	Water level	GRACE, Tropical Rainfall Measuring Mission (TRMM)	Reconstruction and prediction water level
Fok, et al., 2018	Water level	GRACE, Palmer's Severity Index (PDSI), and El Nino Southern Oscillation	Reconstruction water level

		(ENSO) indices	
Lv et al., 2017	Evapotranspiration	GRACE, Global Land Data Assimilation System (GLDAS)	Reconstruction evapotranspiration
Li et al., 2018	Evapotranspiration	GRACE, in situ data	Estimation evapotranspiration
Ferreira et al., 2013	Discharge	GRACE; TRMM; GLDAS	Estimation total discharge
Chen et al., 2019	Discharge	GRACE, TRMM, Moderate Resolution Imaging Spectroradiometer (MODIS)	Estimation total basin discharge and its seasonal error characterization
Zhang et al., 2015	Drought	GRACE	Detection droughts and connections with ENSO
Zhang et al., 2016	Drought	GRACE	Evaluation hydrological drought
Zhou et al., 2017	Drought and flood	GRACE, MODIS	Characterizing drought and flood events
Sun et al., 2018	Drought	GRACE	Evaluation drought
Zhang et al., 2019	Drought	GRACE, and in-situ data	Assessment of hydrological drought and its recovery time
Chao et	Flood	GRACE, hydrological model,	Characterized flood potential

al., 2017b			and in-situ data	
Gao et al., 2017	Flood		GRACE, precipitation	Estimation for flood frequency
Sun et al., 2017	TWS and Flood		GRACE, TRMM	Assessing TWS and flood potential
Huang et al., 2015	TWS changes		GRACE, hydrological model	Estimation of human induced changes in TWS
Long et al., 2015	TWS changes		GRACE, hydrological model	Deriving scaling factors using a global hydrological model to restore TWS
Yang et al., 2018	TWS changes		GRACE, GLDAS, TRMM	Analysis of the spatiotemporal changes in TWS
Li et al., 2019	TWS changes		GRACE	Evaluation the effects of leakage error on TWS changes
Zhang et al., 2019	TWS changes		GRACE, and in-situ data	Evaluation of GRACE mascon solutions for small spatial scales TWS changes
Jiang et al., 2016	Groundwater change		GLDAS; GRACE; satellite altimetry	Monitoring groundwater changes
This Study	Spatiotemporal variability of each		GRACE, hydrological model, satellite altimetry (ICESat,	Characterization each component of TWS changes

component TWS (CryoSat-2), MODIS, precipitation (P), evapotranspiration (ET), and in situ of P, ET, runoff, surface water level data

**Table 2**

Basic information of data sources used in this study. Note: TWS, terrestrial water storage; SH, spherical harmonic; ET, evapotranspiration; P, precipitation; R, runoff; SMS, soil moisture storage.

Component	Description	Resolution	Time span	Sources
TWS	GRACE SH	Monthly	/ 2002-2	<a href="http://icgem.gfz-potsdam.de/ICGEM/shms/monthly">http://icgem.gfz-potsdam.de/ICGEM/shms/monthly</a>
	and Mascon solutions	1°×1°	015	<a href="ftp://podaac.jpl.nasa.gov/allData/tellus/L3/mascon/">ftp://podaac.jpl.nasa.gov/allData/tellus/L3/mascon/</a>
P	TRMM	Monthly	/ 2002-2	<a href="https://disc2.gesdisc.eosdis.nasa.gov/data/TRMM_L3/TRMM_3B43.7/">https://disc2.gesdisc.eosdis.nasa.gov/data/TRMM_L3/TRMM_3B43.7/</a>

		Monthly	/	2002-2	<a href="http://www.esrl.noaa.gov/psd/data/gridded/data.gp">http://www.esrl.noaa.gov/psd/data/gridded/data.gp</a>
	GPCP				
		2.5°×2.5°		016	<a href="#">cp.html</a>
ET		Monthly	/	2003-2	<a href="https://modis.gsfc.nasa.gov/data/">https://modis.gsfc.nasa.gov/data/</a>
	MODIS				
		2.5°×2.5°		013	
Glacier	CryoSat-2			2010-2	<a href="https://science-pds.cryosat.esa.int/#">https://science-pds.cryosat.esa.int/#</a>
		/			
elevation				016	
change	ICESat			2003-2	<a href="https://n5eil01u.ecs.nsidc.org/GLAS/">https://n5eil01u.ecs.nsidc.org/GLAS/</a>
		/ 91 day			
				009	
	SRTM	/			<a href="http://srtm.csi.cgiar.org/srtmdata/">http://srtm.csi.cgiar.org/srtmdata/</a>
				2000	
		3-arc-second			
Lake	Topex/Poseidon,				
water					
level	Jason-1/2,			2003-2	
	--				<a href="http://hydroweb.theia-land.fr/hydroweb">http://hydroweb.theia-land.fr/hydroweb</a>
change	GFO,			015	
	ERS-2 and				
	Envisat				
<b>Land surface models</b>					
P, ET, R,	GLDAS-1(C				<a href="http://disc.sci.gsfc.nasa.gov/services/grads-gds/gld">http://disc.sci.gsfc.nasa.gov/services/grads-gds/gld</a>
		Monthly	/	2002-2	
SMS,	LM, MOS,				as
		1°×1°		016	
TWS	NOAH, VIC)				
	CLM4.0	Monthly	/	2003-2	<a href="https://www.earthsystemgrid.org/">https://www.earthsystemgrid.org/</a>

		0.9°×1.25°	015	
		Monthly	/	2002-2 <a href="https://www.uni-frankfurt.de/45218063/WaterGAP">https://www.uni-frankfurt.de/45218063/WaterGAP</a>
	WGHM			
		0.5°×0.5°	012	
<b>Ground-based observation</b>				
Hydrolog			2003-2	<a href="http://www.cjw.gov.cn/">http://www.cjw.gov.cn/</a>
	Datong	Monthly		
ical			015	
stations			2003-2	
	Hukou	Monthly		
(P, ET,			013	
R, and			2003-2	
	Chenlingji	Monthly		
water			013	
level)			2003-2	
	TGR	Daily		
			016	
Weather	China			<a href="http://data.cma.cn">http://data.cma.cn</a>
stations	Ground			
(P and	Climate		2003-2	
		Daily		
ET)	daily		013	
	observation			
	Data			

Table 3

Trends of TWS changes and its individual components during 2003–2015.

R	G	T	O	D	P	O	S	T	H	C	T
		GRI	thers	oting	oyan	thers					
esults	MC	Total RI	RI	L	g	Lake	M	GWS	GWS	GWS	WS
				ake	Lake	s					
				Total LWS							
				SWS							
T											
WS											
chang											
e and											
its											
individ	-0.06	0.37±	0.03±	0.12±	0.06±	-0.02	1.65±	10.39	4.87±	5.54±	12.04
ual	±0.04	0.15	0.01	0.04	0.05	±0.01	0.88	±1.27	1.12	1.02	±1.81
compo											
nents											
(Gt											
yr-1)											

**Table 4**

Correlation coefficients between the P, ET, R, TWS, GMC, TGR, Poyang Lake, Doting Lake, SM, TGWS, and HGWS with p-value < 0.001 from the monthly time series during 2003–2013.

Note: TGR refers to the water level change in the TGR.

Correlation coefficients	P	ET	R	TWS	GMC	TGR	Poyang	Doting	SM	TGWS	HGWS
P	1	0.73	0.69	0.38	-0.41	-0.23	0.75	0.63	0.44	0.24	0.09
ET		1	0.74	0.44	-0.33	-0.23	0.68	0.50	0.35	0.35	0.16
R			1	0.71	-0.28	-0.19	0.86	0.71	0.70	0.52	0.22
TWS				1	-0.51	0.37	0.62	0.58	0.65	0.90	0.66
GMC					1	0.03	-0.11	-0.21	-0.03	-0.07	-0.01
TGR						1	-0.17	-0.01	-0.16	0.55	0.65
Poyang							1	0.69	0.65	0.42	0.18
Doting								1	0.54	0.41	0.16
SM									1	0.28	-0.01
TGWS										1	0.84
HGWS											1

- TWS change in the YRB is derived using LMM and validated using in situ data.
- Each components contribution to TWS change in the YRB is quantified.
- The relationship between each component of TWS change is investigated.
- The CryoSat-2/ICESat are combined to monitor the glacier mass change.

Journal Pre-proofs